Articles in PresS. J Neurophysiol (May 11, 2016). doi:10.1152/jn.00116.2016

Recording extracellular neural activity in the behaving monkey using a semi-chronic and high-density electrode system

Germán Mendoza[1], Adrien Peyrache[2], Jorge Gámez[1], Luis Prado[1], György Buzsáki[2] and Hugo Merchant[1*]

[1]*Instituto de Neurobiología, UNAM, Campus Juriquilla, México.*

[2]*The Neuroscience Institute, School of Medicine and Center for Neural Science, New York University, New York, NY 10016, US*

Running title: High-density electrode system for recordings in monkeys

*To whom correspondence should be addressed: Dr. Hugo Merchant, Phone: 442-238-1040 E-mail: hugomerchant@unam.mx

Abstract

We describe a technique to semi-chronically record the cortical extracellular neural activity in the behaving monkey employing commercial high-density electrodes. After the design and construction of low cost microdrives that allows varying the depth of the recording locations after the implantation surgery, we recorded the extracellular unit activity from pools of neurons at different depths in the presupplementary motor cortex (pre-SMA) of a Rhesus monkey trained in a tapping task. The collected data was processed to classify cells as putative pyramidal cells or interneurons on the basis of their waveform features. We also demonstrate that short time cross-correlogram occasionally yields unit pairs with high short latency (<5 msec), narrow bin (<3 msec) peaks, indicative of monosynaptic spike transmission from pre to postsynaptic neurons. These methods have been verified extensively in rodents. Finally, we observed that the pattern of population activity was repetitive over distinct trials of the tapping task. These results show that the semi-chronic technique is a viable option for the large-scale parallel recording of local circuit activity at different depths in the cortex of the macaque monkey and other large species.

New & Noteworthy

This paper demonstrates high density, chronic recordings of single units at different depths in behaving monkeys, which have been achieved until now only in rodents. We also show how two, and potentially many, silicon probes can be implanted effectively and at low cost in primates. Using different analytical tools on simultaneously recorded cells, we were able to identify inhibitory and principal cells, so that functionally connected cortical assemblies can be studied during task performance.

Introduction

Brain function is the result of the structured interaction of groups of neurons forming functional networks in time and space (Mountcastle 1995; Buzsáki 2010). Recording of the extracellular activity of few neurons during different conditions or tasks has been a useful tool for the study of neuronal function in distinct brain areas (Mountcastle et al. 1969, 1975; Andersen et al 1985; Georgopoulos et al. 1986; Schultz and Romo 1992; Lebedev et al. 2000). In those studies, the limited number of simultaneously recorded neurons and the variability of the neuronal responses as a function of the task parameters impose the necessity of collecting many trials under the same condition to determine the statistics of the neural response (Brown et al. 2004). This experimental strategy, however, results in a limited description of the functional properties of single cells, neural populations, and the dynamic interactions of different types of neurons (i.e., pyramidal versus fast spiking interneurons [FS]) forming anatomic-functional networks (Merchant et al., 2012). In contrast, the brain processes information on a trial-by-trial basis exploiting the population activity to represent different behavioral parameters (Quian Quiroga and Panzeri 2009). Thus, the comprehension of the mechanisms that make brain function possible requires the simultaneous sampling of the activity of representatively large groups of neurons (Brown et al. 2004; Buzsaki et al. 2015; Nicolelis and Lebedev 2009). Recent technological innovations have allowed the simultaneous recording of large number of neurons in several cortical and subcortical regions of the brain of awake, behaviorally trained rodents and nonhuman primates (Berényi et al. 2014; Dotson et al. 2015; Fraser and Schwartz 2012; Hatsopoulos and Donoghue 2009; Schwarz et al. 2014; Vandecasteele et al. 2012). Such methods and their combination with optogenetic tools have result in a better understanding of the brain function (Buzsáki et al. 2015; Wu et al. 2013, 2015). In spite of such progress, large-scale recordings are still technically challenging, have not been generalized across animal models, and each method has its own pros-and-cons. For example, a widely used method for chronic multiple recordings in human and non-human primates is the Utah array that has a 10 by 10 matrix arrangement (Schmidt et al. 1993). However, this FDA approved recording system can only explore the functional properties of cell populations in the exposed flat part of the cortical gyri, with a maximum depth of 3 mm, and with no option to modify the recording location once placed. Furthermore, the 100 electrodes, each with a width of 80 μm can have a deleterious effect on the horizontal connections of the cortical tissue and its normal functioning (Ward et al. 2009).

The aim of the present study was to adapt a technique developed recently for the large-scale recording of extracellular activity in behaving rodents (Vandecasteele et al. 2012) to neural recordings in the behaving monkey. Nonhuman primates have been useful animal models for cognitive neuroscience for long time (Evarts 1968; Mountcastle et al., 1969) due to the similarity of their neuroanatomy and body plan to that of humans, and the possibility to train them in a variety of complex motor, perceptual and cognitive tasks not available in other animal models (Averbeck et al., 2002; Crowe et al., 2004; Merchant et al., 2004a, 2004b; Chafee et al., 2007;

Merchant et al., 2011a; Mendez et al., 2011). We employed commercial micromachined electrode arrays (NeuroNexus, MI, USA, http://www.neuronexus.com) for high-density recording of neuronal activity in the presupplementary motor cortex (pre-SMA) of a Rhesus monkey working in a tapping task, which has been a backbone paradigm in the study of the neural basis of beat perception and entrainment (Zarco et al. 2009; Merchant et al. 2011b; Merchant et al. 2015a). To achieve this, we developed a compact, low-cost microdrive, robust enough for semi-chronic recordings in the monkey. The technique allowed the recording of extracellular activity of local populations of neurons at different cortical depths during several weeks. Interestingly, we observed that the population activity was repetitive over distinct trials of the tapping task. Moreover, it was possible to identify monosynaptic connections between neurons and to classify them as putative pyramidal or interneurons. Such information was employed for the description of the functional connectivity in local circuits (Barthó et al. 2004). These results show that our method is a viable option for the chronic recording of local circuit activity in the cortex of the monkey and other large species. Current experiments employing this technique in our laboratory will provide new insights on the neurophysiology of explicit time processing by nonhuman primates.

Materials and methods

System Description

We adapted the technique employed by Buzsáki and coworkers for semi-chronic recordings in rodents (Berényi et al. 2014; Vandecastele et al. 2012) to similar recordings in the behaving monkey. We used the Buzsaki64-Z64 probe manufactured by NeuroNexus (http://www.neuronexus.com). Nevertheless, other probes with similar structural characteristics can be employed (for an extensive comparison of the performance of several commercial probes chronically implanted in rodents review the work of Ward et al. 2009). The probe consists of 8 silicon shanks separated from each other by 200 μm each with 8 recording sites located at intervals of 20 μm in the vertical axis (Figure 1A). The probe was connected to a microdrive that allowed the control of the movement of the probe in the dorso-ventral axis. Our microdrive consists of a body, a shuttle, and a basis (Fig. 1B). For the construction of the body and the shuttle electrical bakelite circuit board and board-to-board connectors (gold plated, pitch spacing: 2.54 mm, Smatec, www.samtec.com) were employed. The probe was fastened to the microdrive shuttle with dental acrylic. In addition, a brass screw (00-90 x 1, Fasteners & Metal Products Corp. MA, USA, www.fastmetalproducts.com) attached to the body of the microdrive, went through the shuttle giving mobility to the probe. One turn of the screw corresponded to 280 micrometers. The probe, microdrive, and recording connectors were covered by a protective aluminum/stainless steel case when the monkey was not in a recording session (Fig. 3G).

It is possible to modify the basic structure of the microdrive in order to meet the needs of a particular experiment. The micromanipulator can be redesigned to accommodate different number of probes, different electrode configurations, recording locations, and recording depths. Importantly, these adaptations can be done in the laboratory employing commonly available tools and materials. For example, Figure 1D shows a modification of the microdrive described above (Figure 1B). The microdrive consists of two Buzsaki64-HZ64 probes glued to two shuttles mounted in the same body (Figure 1D). Each shuttle is totally independent and is moved by a single screw. The microdrive allows the independent insertion and movement of the two probes in the same or in closely adjacent cortical areas. The two shank arrays were mounted 4 mm apart, but different distances can be achieved. Furthermore, the microdrive, the probe connectors and the reference and ground connectors were attached in the same platform, conforming a single mechanically robust module. This design results in compact implants (Fig. 4C) and reduces substantially the time required for implanting the probes and the overall surgery duration. A critical aspect for long-term recordings (up to 74 days so far, see Table 1) is the utilization of probes that includes a polyamide cable that connects the shank array with the probe connector (Fig. 1C). The polyamide cable and the use of the 64-channel ZIP-Clip connector (Tucker-Davis-Technologies, http://www.tdt.com) permit the easy day-by-day connection of the headstages without transferring force to the implanted electrodes and the surrounding tissue.

Preparing the shanks for the implantation

Prior to surgery, it was important that the headstages and the ZIP-Clip probe connector mate smoothly, avoiding excessive force to connect them. When this condition was not met, we employed a scalpel to cut small amounts of the probe connector until an easy mating was achieved. Next, the probe recording sites were cleaned in a solution of 4% of Conrad detergent (Conrad 70, Decond) in distilled water at 63° Celsius during 2 hours. Subsequently, the detergent was removed by the repeated immersion of the silicon shanks in distilled water (Vandecastele et al. 2012). Just before surgery, the probes as well as the microdrive were disinfected with 70% alcohol. In our experience, this method effectively avoided implant infections. Alternatively, sterilization can be achieved with oxide ethylene gas (Oliveira and Dimitrov, 2008).

Surgical procedures

All the animal care, housing, and experimental procedures were approved by the National University of Mexico Institutional Animal Care and Use Committee and conformed to the principles outlined in the Guide for the Care and Use of Laboratory Animals (NIH, publication number 85-23, revised 1985). One male Rhesus monkey (8.5 kgs) was subjected to two implantation procedures separated by 10 months. In the first procedure, one 64-channel probe was implanted in the right pre-SMA, whereas in the second two probes were simultaneously implanted in the left and right pre-SMA.

Skullcap construction

The monkey was anesthetized initially with an intramuscular dose of ketamine (7 mg/kg)-xylazine (0.6 mg/kg), then underwent endotracheal intubation for sevofluorane anesthesia, and mounted on the stereotaxic apparatus. After preparing the skull vertex area (see Oliveira and Dimitrov, 2008), we localized the stereotaxic coordinates of the recording sites based on structural MRI (high-resolution T1-weighted gradient echo sequence, TR = 20 ms, TE = 6.9 ms, flip angle = 25°, matrix = 240 x 108, slices = 80, resolution = 1.0 mm x 1.0 mm x 1.0, on a 3.0 T Philips MRI Scanner, Merchant et al., 2011b). Subsequently, we attached to the cranium the reference and ground screws/wires, as well as the titanium posts for head fixation and the securing screws (Fig. 2A). The securing screws and the basis of the titanium posts were covered with dental acrylic. Once the dental acrylic was hardening but still malleable, we built a flat acrylic platform (4.5 cm of diameter) around the recording site for the future fixation of the microdrive and the protective case (Fig. 2B). The reference and ground gold pins should protrude 7 mm over the implant surface (Fig 2C,D). After the dental acrylic was cured, antibiotic ointment was applied on the wounds. The monkey was retired from stereotaxic frame and allowed to recover in a quiet room. Broad spectrum antibiotics (Enrofloxacin, 5 mg/kg/day) and analgesics

(Ketorolac 0.75 mg/kg/6 hrs. or Tramadol 50-100 mg/4-6 hrs.) were administered intramuscularly the day of the surgery and in two subsequent days.

Probe implantation

The monkey was retrained in tapping task (Zarco et al., 2009; Merchant and Honing 2014) with its head fixed in the head-holding device. Then a second surgery was performed in order to implant the shank array. Anesthetic and aseptic methods were the same to those of the first surgery. First, with the monkey fixed on the stereotaxic frame, a craniotomy was drilled through the acrylic skull cap and skull in the previously identified stereotaxic coordinates (Figure 3A). Next, the dura matter at the insertion point was opened employing a miniature surgical blade or a hook (Vandecasteele et al. 2012). The microdrive was mounted in a stereotaxic tower for the positioning of the shanks (see Vandecasteele et al. 2012). Once the shanks were aligned with the penetration site, the microdrive was attached to the head cap by means of titanium screws and dental acrylic (Fig. 3B, 4B). Notably, the alignment of the shank array and the craniotomy and dura dissection point must be verified before fixing the microdrive in place. Once the microdrive was firmly attached to the skullcap, the stainless steel ring was mounted employing titanium screws and dental acrylic (Fig. 3C, 4C). We moved the microdrive screw to penetrate the shanks into the cortex under microscope assistance. We did not see brain dimpling during electrode insertion. Instead, the shanks may be bent due to their thin section (15 μm width) and flexibility. Consequently, care must be taken to avoid bending shanks excessively, because they can brake (Fig. 3D, Vandecasteele et al. 2012). If the shanks bent, they were pulled-up and then the penetration was tried again until the recording sites were inserted in the superficial layers of the cortex. Once the electrodes were implanted, the craniotomy was closed with a warm mixture of paraffin/mineral oil applied with a sterile syringe (Fig. 3F, 4C). After the presence of neural activity was verified, the aluminum case was placed to protect the probes, microdrive, and connectors (Fig. 3G). Antibiotic and analgesics were administered as in the first surgery.

Implant maintenance

After the implantation surgery care was taken to maintain the microdrive and the probe connectors clean from the cerebrospinal fluid and other debris that leaked from the craniotomy. Daily cleaning of the paraffin seal, the microdrive, and the probe connectors with sterile cotton swabs prevented implant infections and diminished recording artifacts that can result from humid probe connectors. Persistent humidity was eliminated with compressed air. Especially dirty connectors were cleaned with the point of a sterile syringe needle or with a sterile miniature brush under a surgical microscope view.

Signal acquisition

The neural data of 64 or 128 channels was acquired, amplified, and digitized using a PZ2 preamplifier (Tucker-Davis Technologies, FL, USA, http://www.tdt.com) at 24,414Hz. The signal was transmitted to a RZ2 base station through fiber optic for on-line processing.

Spike detection and discrimination

Raw recording traces were high-pass filtered at 800 Hz and action potential candidates were selected as any events larger than seven standard deviations above baseline on at least one of the channels from the electrode group (the eight channels of a given shank on the silicon probe). Spike sorting was then performed semi-automatically, using KlustaKwik (Harris, et al., 2000; available at: http://klusta-team.github.io/klustakwik/) after dimensionality reduction of the waveforms using standard principal component analysis (three components per channel typically explaining almost all the variance). This was followed by the manual adjustment of the waveform clusters using the software Klusters (Hazan, et al., 2006). In one session, up to 64 isolated single neurons were detected (average of 27 cells per recording, range: 9-64 cells, for four analyzed recording sessions).

Identification of monosynaptic connections

Pairwise cross-correlations between all possible pairs of simultaneously recorded neurons were calculated using the discharge rate of cells in 0.5ms bins. Cross-correlograms were smoothed with a 5 ms standard deviation Gaussian kernel (which is equivalent to a jittering of the spikes from the two neurons). At each time bin, the interval of confidence of the smoothed cross-correlogram was evaluated as the 99.9th percentile of a Poisson process defined by the rate resulting from the smoothing procedure (Stark and Abeles, 2005). A putative excitatory or inhibitory connection was considered when any two consecutive bins of the original cross-correlogram exceeded the interval of confidence between 0 and 8ms. The cross-correlograms were then manually examined to remove any spurious connections.

Results

System description

We customized the large-scale system used to record from multiple single units in behaving rodents in order to use the same methodological and analytical framework in monkeys performing different paradigms. We used the Buzsaki64-Z64, which consists of eight silicon shanks each with eighth staggered recording sites separated vertically by 20 μm (Figure 1A). Furthermore, we modified the system to allow the independent recording of two separate but adjacent cortical areas with two probes. Each probe was coupled to a microdrive that allowed the independent control of the recording position in dorso-ventral axis (Figure 4). With this system, we had the possibility to perform large-scale recordings in deep cortical areas in the profound gyri (up to 5mm) for more than 10 consecutive weeks (see Table 1). Figure 5A shows the wide-band signal of the eight recording sites of one of the inserted shanks in the supplementary motor cortex of a Rhesus monkey. The same neuron could be recorded in different recording sites of one shank, as illustrated in Figure 5B, where the raster of seven spikes of the corresponding action potentials on the Figure 5A is shown with the same color code. Thus, the voltage profile of spikes across the recording sites in a probe provided an approximate location of the cell body of the recorded neuron (Csicsvari et al. 2003).

Unit clustering

Spike detection, feature extraction, and spike discrimination using clustering methods was performed semi-automatically with the open-source software KlustaKwik (Harris, et al., 2000). Spike clusters were manually adjusted and eventually followed standard quality criteria such as low level of refractory period contamination. Figure 6A shows the spike clusters of the seven cells depicted in Figure 5 using the same color code. These clusters are displayed along the first principal components of spike waveforms extracted from the 6^{th} and 7^{th} recording sites. In addition, Figure 6B illustrates the mean (± standard deviation) of the waveform of the seven-clustered cells (spk1-spk7, same color code) across the eight neighboring recording sites (RS1-RS8) of one silicon probe. The analysis of the auto- and cross-correlograms, depicted in Figure 6C also provided valuable information for the spike discrimination process. The diagonal of auto/cross-correlogram matrix (Fig. 6C) corresponds the auto-correlograms for the same seven cells (in color code Fig 6A,B). These auto-correlograms showed an absence of spikes at short intervals (<2 ms) corresponding to the refractory period of the neurons and thus indicating that the recording of each of the seven spikes was made from a single independent cell. Furthermore, asymmetric peaks in the cross-correlograms can indicate that the decreasing amplitude of the spikes within a burst produced by a single cell have been classified as a separate cluster (Harris et al., 2000). However, Figure 6C shows that all cross-correlograms (gray) were symmetric, supporting the notion of robust spike discrimination.

Large-scale recording from multiple single units in the behaving monkey

A monkey was trained to synchronize its hand taps to a button with a sequence of pacing isochronous visual stimuli. The animal developed a timing behavior that was built from the predictive rhythmic structure of the task (Merchant et al., 2008, 2013). Interestingly, the silicon probe recordings during task execution showed that the periodic taping of the monkey was associated with a repetitive pattern of activation of multiple single cells. Figure 7A shows the simultaneous recording of sixty-four cells that were sorted by their response onset latency. It is evident that the neurons show many cycles of activations and that the phase of this activations changed systematically across the neuronal population, forming a neural avalanche of activation on every task trial. The repetitive pattern of activity could be clearly observed by projecting the ensemble profile of activation overtime onto the first two principal components. As seen on Fig. 7B, the population activity is, in this principal component subspace, rotating cyclically along a low-dimensional trajectory. Indeed, the trial-by-trial analysis of the population neural trajectories, depicted in Figure 7C, show a stereotypic behavior where the neural dynamics start in the middle lower part of the PCA subspace (dark blue), then rotates counterclockwise to finally return around the initial starting point (yellow colors). Interestingly, the cyclical trajectories are similar for trials where the monkey produced intervals with different durations, suggesting a relative rather than an absolute representation of the passage of time. A similar phenomenon was observed in single neuron and ensemble activity recorded in the primary motor and premotor cortices of monkeys producing self-timed hand movements (Lebedev et al., 2008). Furthermore, the population neural trajectories were similar in trials where the monkey did not tap and only perceived the sensory metronome (Figure 7C, trial 15). These phenomena were already documented in a tapping task but using the activity of pre-SMA neurons recorded in many different sessions due to the small number of simultaneously recorded cells (Merchant el al., 2014a; Crowe et al., 2014; Merchant et al., 2015b). Hence, the simultaneous recordings of hundreds of cells in a particular cortical area during complex cognitive tasks will allow the characterization of neural population codes that can be related with different parameters of behavior on a trial-by-trial basis.

Electrophysiological and functional identification of pyramidal and fast spiking (FS) neurons

Units were classified as putative pyramidal cells and putative GABAergic interneurons on the basis of their waveform features. Putative pyramidal cells were characterized by broad waveforms whereas putative interneurons showed narrow spikes (Merchant et al., 2012). To separate between the two classes of cells, we used two waveform features: (i) half-peak duration, which corresponds approximately to the time it takes for the membrane potential to repolarize (ii) the trough-to-peak duration. These two waveform features were clustered using an Expectation-Maximization method fitting the population with a mixture of two two-dimensional Gaussian distributions. Cluster identity of a cell was defined as a posterior probability >80% to

one of the two clusters (Fig. 8A). This method successfully clustered almost all neurons (107/108) which showed clearly separated waveform shape (Fig. 8B). Narrow-spike neurons are likely fast-spiking (FS, and parvalbumin-expressing) interneurons (Royer et al. 2012). As expected, mean firing rates were twice as high for putative FS interneurons than for putative excitatory pyramidal neurons (Fig. 8C; $p < 10^{-4}$, Wilcoxon rank sum test). Many studies have shown that the electrophysiological signatures of extracellular action potentials and the spontaneous activity of the cells cannot be the only criteria to identify putative pyramidal versus putative FS interneurons, due to the large amount of classification errors (Bartho et al., 2004; Merchant et al., 2008; 2012). Thus, one of the large advantages of the silicon probe system used in the present study is its high recording density, which maximizes the possibility to find monosynaptic interactions between multiple pairs of neurons. Consequently, the cell types were further assessed by analyzing candidates of synaptic connection between cell pairs evidenced from their temporal cross-correlogram at millisecond time range (Bartho et al. 2004; Peyrache et al. 2012). Figure 8D shows an example of an excitatory post-synaptic effect of a broad waveform, putative pyramidal neuron onto a narrow-spike, putative FS cell. The average probability of connectivity is 1.45% (+/- 1.25, SD), for a total number of eight excitatory connections.

Discussion

The main novel contributions of our report are: 1) the development of a new compact, low-cost implantable microdrive and its corresponding protective device, both of them robust enough for semi-chronic recordings in the monkey and other large animals; 2) the development of a new implantation technique that, in combination with our microdrive design, saves time during surgeries; 3) these innovations allowed us to perform chronic high-density recordings of extracellular activity of local populations of neurons at different cortical depths during several weeks in the rhesus monkey, which to our knowledge has not previously accomplished; and 4) the demonstration that advanced spike sorting and analytical techniques recently developed for chronic recordings in rodents can be also employed for the analysis of chronic recordings performed in larger animals such as the rhesus monkey.

Our method combines the flexibility of acute recordings, the advantages of chronic systems, the high spatial resolution, and the massive neurophysiological information generated by high-density silicon probes. These features provide our technique with several advantages over previous reported methods. First, in contrast to other chronic, high-density systems like the Utah array, our microdrive allows the movement of the electrode arrays at any time during different recording sessions. The arrays can be moved in the dorso-ventral axis to optimize the recording quality or to scan the properties of deep regions of the cortical tissue. Second, the micromanipulator can be redesigned to accommodate different number of probes, electrode configurations, recording locations, and recording depths. Most important, these adaptations can be done in the laboratory at a very low cost, employing commonly available tools and materials. Third, we employed NeuroNexus commercial probes, but any recording array with similar structural characteristics can be employed. Fourth, the microdrive, the probe connectors and the reference and ground connectors are attached in the same platform and form a single mechanically robust module. This design results in compact implants and reduces substantially the time required for implanting the probes and the overall surgery duration. This is achieved because the spatial relation between the recording probes and all the required connectors is adjusted prior to surgery and all of them are implanted at the same time as a whole after opening the craniotomy. Fifth, the type of probe mounting and connector employed permit the fast and easy day-by-day connection of the head stages without transferring force to the implanted electrodes and the surrounding tissue. Sixth, our recording method can be combined with recently developed freely available spike sorting tools which were specially designed for recordings with high density electrode arrays (Rossant et al. 2016).

On the other hand, one disadvantage of our system is that it requires the daily cleaning of the microdrive and the probe connectors, and to maintain the aseptic conditions of the implant site. In our experience, daily cleaning of the paraffin seal, the microdrive, and the probe connectors prevented implant infections. This procedure also maintained the connectors clean and dry which is a prerequisite to avoid recording artifacts. It is important to mention that these

disadvantages are similar to those presented in classic acute recordings (Naselaris et al., 2005) and that the advantages of our method clearly overcome these drawbacks.

The use of silicon probes with multiple, staggered recording sites allowed the identification of distinct neuronal clusters in the pre-SMA of the behaving monkey that were reliably identified using standard semi-automatic clustering software. Thus, the voltage profile of spikes across the recording sites in a probe provided an approximate location of the cell body of the recorded neuron. Furthermore, we were able to record sixty-four cells simultaneously during the performance of a tapping task. Their activation profile showed many cycles of activations, where the response phase changed systematically across the neuronal population, forming periodic neural avalanches during task performance. In fact, at the population level, a cyclic and systematic trial-by-trial pattern of activation was observed when the ensemble response profile overtime was projected onto the first two principal components. Finally, using different electrophysiological signatures and the cross-correlograms of simultaneously recorded cells, we were able to identify inhibitory interneurons and principal cells in cortical networks. Thus, the parallel recordings of neuronal activity allowed for the identification of anatomically and functionally connected assemblies.

Non-human primates and in particular Rhesus monkeys have been a fundamental animal model in cognitive neuroscience for almost 50 years (Evarts 1968; Mountcastle et al., 1969; Lin et al., 2014). Neurophysiological studies in different brain areas while monkeys perform a variety of perceptual (Britten et al., 1992; Romo and Salinas, 2003), memory- or rule-based (Miller, 2000; Tomita et al., 1999), spatial and temporal cognition (Georgopoulos et al., 1994; Chafee et al., 2007; Seo et al., 2012; Seo et al., 2014, Merchant et al., 2013; Jazayeri and Shadlen, 2015), numerosity (Nieder and Miller, 2003), and fine voluntary motor control tasks (Schwartz 1994; Kraskov et al., 2009; Churchland et al., 2012) are the pillars of system neuroscience. Thus, despite the world-wide pressure to abandon this model, macaques are still a valuable and necessary model for the study of high cognitive processes at the single cell and neural population levels, due to the similarity of their neuroanatomy and general body plan to those of humans, and the possibility to train them in a variety of complex paradigms not available in other animal models. Nevertheless, many monkey neurophysiologist are still using the single electrode approach to study the neural underpinnings of cognition, with a total disregard on how large ensembles of cells interact to process and transfer information between and within brain areas (see Merchant et al., 2014b; Crowe et al., 2013 for some exceptions), and how the anatomy of neural circuits define high-order brain operations. In contrast, different large-scale recording methods have been developed in behaving rodents with enormous success. In particular, the use of silicon-probes for high-density recordings of local circuits in behaving rats and mice have open the possibility for the systematic study of hundreds of simultaneously recorded neurons, the identification of the electroanatomic boundaries of layers and regions in the hippocampus and neocortex, the construction of circuit diagrams of functional connections (excitatory or inhibitory) among neurons in real anatomic space (Buzsaki, 2004; Berenyi et al.,

2014), and the investigation of the circuit operations and behavior-dependent interactions between and within brain areas (Berenyi et al., 2014; Fujisawa et al., 2008). Furthermore, the large-scale recordings of neuronal spiking with silicon probes can be combined with the optogenetic manipulation of the activity of diverse neuronal phenotypes in order to determine the causal role of different circuit components and brain areas on the organization of behavior (Buzsáki et al., 2015). Consequently, the purpose of this study was to adapt the large-scale recording system of behaving rodents to use the same methodological and analytical framework in monkeys executing different paradigms. We were not only successful to record neural activity for many weeks from different depths of pre-SMA in a monkey, but also managed to redesign the recording system and the micromanipulators to accommodate different number of probes, different electrode configurations, recording placements, and recording depths. Such versatility could be useful for the dense recording of multiple interconnected areas during the execution of particular tasks. A promising avenue to identify functional circuits across cortical areas in the monkey is the use of electrical microstimulation of key cortical or subcortical nodes and to measure the induced changes in functional magnetic resonance imaging to evaluate the functional activity resulting from the stimulation of interconnected regions (Tolias et al., 2005; Moeller et al., 2008; Petkov et al., 2015) or optogenetic stimulation of neurons (Wu et al. 2013, 2015). Thus, once the interconnected voxels are identified in a specific macaque, the employment of the semi-chronic system described here will allow the study of the critical processing nodes linked to a high order behavior with all the mentioned methodological strengths that have the high-density recordings with silicon probes.

The geometrically precise distribution of the eight recording sites across eight silicon shanks allowed for robust spike discrimination using semi-automatic clustering software, since the signal coming from one neuron can be recorded in adjacent recording sites. The semi-automatic process consisted of an automatic classification program that uses the information of all recording sites, followed by examination and reassignment by a human operator. Therefore, the semi-automatic spike sorting is considerably faster than the manual method, is free from the subjective bias and the experience level of the experimenter, and show lower error rates in spike discrimination (Harris et al., 2000). In addition, the 2D recording arrangement of the silicon probes permit the determination of the “center of mass”, i.e., the approximate two-dimensional position of cell bodies of the putative single neurons with respect to the electrode layout (Csicsvari et al., 2003). This is the first step for the partial circuit reconstruction based on physiological interactions. Second, the dense recording distribution maximizes the probabilities to find monosynaptic excitatory and inhibitory interactions between pairs of cells, which are characterized by large peaks or troughs at short-latency time lags in the cross-correlograms. With spatially closely recorded neurons, it is possible to determine the monosynaptic connections between cells. Third, using the spike duration and the spontaneous discharge rate of the cells it is possible to identify putative pyramidal, with long duration action potentials and low discharge rate, and putative FS interneurons, with narrow action potentials and high discharge rate (Merchant et al., 2008). This information can complement the partial circuit reconstruction

based on determination of the monosynaptic connections. Finally, dynamics in the interactions between cellular elements of the partially reconstructed network can be determined as a function of different task epochs and the value of the independent parameters of a specific behavioral paradigm (Fujisawa et al., 2008). Indeed, graph theory is a promising tool to identify how the reconstructed small circuit interactions change as a function of behavior (Carrillo-Reid et al., 2011).

In summary, large-scale recordings of single units with silicone-probe systems allows for a detailed study of the neural correlates of complex behaviors in the behaving monkey at many levels of neural processing: single cells, cell populations, the interaction between different cell types and their position across layers and cortical columns, functional circuits, as well as the interplay between encoding of behavioral parameters in the action potentials with the dynamic oscillations in different frequency bands on the surrounding cerebral tissue.

Acknowledgements

We thank Raul Paulín for his technical assistance. Supported by CONACYT: 236836, PAPIIT: IN201214-25 grants to H. Merchant, CONACYT scholarship 164310 to G. Mendoza, and National Institute of Health grants NS34994, MH54671, and NS074015 to G. Buzsáki.

References

Andersen RA, Essick GK, Siegel RM. Encoding of spatial location by posterior parietal neurons. Science. 230: 456-458, 1985.

Averbeck BB, Chafee MV, Crowe DA, Georgopoulos AP. Parallel processing of serial movements in prefrontal cortex. Proc Natl Acad Sci USA. 99: 13172-13177, 2002.

Barthó P, Hirase H, Monconduit L, Zugaro M, Harris KD, Buzsáki G. Characterization of neocortical principal cells and interneurons by network interactions and extracellular features. J Neurophysiol. 92: 600-608, 2004.

Berényi A, Somogyvári Z, Nagy AJ, Roux L, Long JD, Fujisawa S, Stark E, Leonardo A, Harris TD, Buzsáki G. Large-scale, high-density (up to 512 channels) recording of local circuits in behaving animals. J Neurophysiol. 111: 1132-1149, 2014.

Britten KH, Shadlen MN, Newsome WT, Movshon JA. The analysis of visual motion: a comparison of neuronal and psychophysical performance. J Neurosci. 12: 4745-4765, 1992.

Brown EN, Kass RE, Mitra PP. Multiple neural spike train data analysis: state-of-the-art and future challenges. Nat Neurosci. 7: 456-461, 2004.

Buzsáki G. Large-scale recording of neuronal ensembles. Nat Neurosci. 7: 446-451, 2004.

Buzsáki G. Neural syntax: cell assemblies, synapsembles, and readers. Neuron. 68: 362-385, 2010.

Buzsáki G, Stark E, Berényi A, Khodagholy D, Kipke DR, Yoon E, Wise KD. Tools for probing local circuits: high-density silicon probes combined with optogenetics. Neuron. 86: 92-105, 2015.

Carrillo-Reid L, Hernández-López S, Tapia D, Galarraga E, Bargas J. Dopaminergic modulation of the striatal microcircuit: receptor-specific configuration of cell assemblies. J Neurosci. 31: 14972-14983, 2011.

Chafee MV, Averbeck BB, Crowe DA. Representing spatial relationships in posterior parietal cortex: single neurons code object-referenced position. Cereb Cortex. 17: 2914-2932, 2007.

Churchland MM, Cunningham JP, Kaufman MT, Foster JD, Nuyujukian P, Ryu SI, Shenoy KV. Neural population dynamics during reaching. Nature. 487: 51-56, 2012.

Crowe DA, Chafee MV, Averbeck BB, Georgopoulos AP. Neural activity in primate parietal area 7a related to spatial analysis of visual mazes. Cereb Cortex. 14: 23-34, 2004.

519 Crowe DA, Goodwin SJ, Blackman RK, Sakellaridi S, Sponheim SR, MacDonald III AW,
520 Chafee MV. Prefrontal neurons transmit signals to parietal neurons that reflect executive control
521 of cognition. Nat Neurosci. 16: 1484-1491, 2013.

522 Crowe DA, Zarco W, Bartolo R, Merchant H. Dynamic representation of the temporal and
523 sequential structure of rhythmic movements in the primate medial premotor cortex. J Neurosci.
524 34: 11972-11983, 2014.

525 Csicsvari J, Henze DA, Jamieson B, Harris KD, Sirota A, Barthó P, Wise KD, Buzsáki G.
526 Massively parallel recording of unit and local field potentials with silicon-based electrodes. J
527 Neurophysiol. 90: 1314-1323, 2003.

528 Dotson NM, Goodell B, Salazar RF, Hoffman SJ, Gray CM. Methods, caveats and the future of
529 large-scale microelectrode recordings in the non-human primate. Front Syst Neurosci. 9:149,
530 2015.

531 Evarts EV. A technique for recording activity of subcortical neurons in moving animals.
532 Electroencephalogr Clin Neurophysiol, 24: 83-86, 1968.

533 Fraser GW, Schwartz AB. Recording from the same neurons chronically in motor cortex. J
534 Neurophysiol. 107: 1970-1978, 2012.

535 Fujisawa S, Amarasingham A, Harrison MT, Buzsáki G. Behavior-dependent short-term
536 assembly dynamics in the medial prefrontal cortex. Nat Neurosci. 11: 823-833, 2008.

537 Georgopoulos AP, Lurito JT, Petrides M, Schwartz AB, Massey JT. Mental rotation of the
538 neuronal population vector. Science. 243: 234-236, 1994.

539 Georgopoulos AP, Schwartz AB, Kettner RE. Neuronal population coding of movement
540 direction. Science. 233: 1416-1419, 1986.

541 Harris KD, Henze DA, Csicsvari J, Hirase H, Buzsáki G. Accuracy of tetrode spike separation as
542 determined by simultaneous intracellular and extracellular measurements. J Neurophysiol. 84:
543 401–414, 2000.

544 Hatsopoulos NG, Donoghue JP. The science of neural interface systems. Annu Rev Neurosci.
545 32: 249-266, 2009.

546 Hazan L, Zugaro M, Buzsáki G. Klusters, NeuroScope, NDManager: A free software suite for
547 neurophysiological data processing and visualization. J Neurosci Methods. 155: 207–216, 2006.

548 Jazayeri M, Shadlen MN. A neural mechanism for sensing and reproducing a time interval. Curr
549 Biol. 25: 2599-2609, 2015.

Kraskov A, Dancause N, Quallo MM, Shepherd S, Lemon RN. Corticospinal neurons in macaque ventral premotor cortex with mirror properties: a potential mechanism for action suppression? Neuron. 64: 922-930, 2009.

Lebedev MA, Mirabella G, Erchova I, Diamond ME. Experience-dependent plasticity of rat barrel cortex: redistribution of activity across barrel-columns. Cereb Cortex. 10: 23-31, 2000.

Lebedev MA, O'Doherty JE, Nicolelis MA. Decoding of temporal intervals from cortical ensemble activity. J Neurophysiol. 99: 166-186, 2008.

Lin CP, Chen YP, Hung CP. Tuning and spontaneous spike time synchrony share a common structure in macaque inferior temporal cortex. J Neurophysiol. 112: 856-869, 2014.

Mendez JC, Prado L, Mendoza G, Merchant H. Temporal and spatial categorization in human and non-human primates. Front Integr Neurosci. 5: 50, 2011.

Merchant H, Bartolo R, Pérez O, Méndez JC, Mendoza G, Gámez J, Yc K, Prado L. Neurophysiology of timing in the hundreds of milliseconds: multiple layers of neuronal clocks in the medial premotor areas. Adv Exp Med Biol. 829: 143-154, 2014a.

Merchant H, Battaglia-Mayer A, Georgopoulos AP. Neural responses during interception of real and apparent circularly moving stimuli in motor cortex and area 7a. Cereb Cortex. 14: 314-331, 2004a.

Merchant H, Crowe DA, Fortes AF, Georgopoulos AP. Cognitive modulation of local and callosal neural interactions in decision making. Front Neurosci. 8: 245, 2014b.

Merchant H, Crowe DA, Robertson MS, Fortes AF, Georgopoulos AP. Top-down spatial categorization signal from prefrontal to posterior parietal cortex in the primate. Front Syst Neurosci. 5: 69, 2011a.

Merchant H, de Lafuente V, Peña F, Larriva-Sahd J. Functional impact of interneuronal inhibition in the cerebral cortex of behaving animals. Prog Neurobiol, 99: 163-178, 2012.

Merchant H, Fortes AF, Georgopoulos AP. Short-term memory effects on the representation of two-dimensional space in the rhesus monkey. Anim Cogn. 7: 133-143, 2004b.

Merchant H, Grahn J, Trainor L, Rohrmeier M, Fitch WT. Finding the beat: a neural perspective across humans and non-human primates. Philos Trans R Soc Lond B Biol Sci. 370: 20140093, 2015a.

Merchant H, Honing H. Are non-human primates capable of rhythmic entrainment? Evidence for the gradual audiomotor evolution hypothesis. Front Neurosci. 7:274, 2014.

Merchant H, Naselaris T, Georgopoulos AP. Dynamic sculpting of directional tuning in the primate motor cortex during three-dimensional reaching. J Neurosci. 28: 9164-9172, 2008.

Merchant H, Pérez O, Bartolo R, Méndez JC, Mendoza G, Gámez J, Yc K, Prado L. Sensorimotor neural dynamics during isochronous tapping in the medial premotor cortex of the macaque. Eur J Neurosci. 41: 586-602, 2015b.

Merchant H, Pérez O, Zarco W, Gámez J. Interval tuning in the primate medial premotor cortex as a general timing mechanism. J Neurosci. 33: 9082-9096, 2013.

Merchant H, Zarco W, Perez O, Prado L, Bartolo R. Measuring time with multiple neural chronometers during a synchronization-continuation task. Proc Natl Acad Sci U S A. 108: 19784-19789, 2011b.

Miller EK. The prefontral cortex and cognitive control. Nat Rev Neurosci. 1: 59-65, 2000.

Moeller S, Freiwald WA, Tsao DY. Patches with links: a unified system for processing faces in the macaque temporal lobe. Science. 320: 1355-1359, 2008.

Mountcastle V. The evolution of ideas concerning the function of the neocortex. Cereb Cortex, 5: 289-295, 1995.

Mountcastle VB, Lynch JC, Georgopoulos A, Sakata H, Acuna C. Posterior parietal association cortex of the monkey: command functions for operations within extrapersonal space. J Neurophysiol. 38: 871-908, 1975.

Mountcastle VB, Talbot WH, Sakata H, Hyvarinen J. Cortical neuronal mechanisms in flutter-vibration studied in unanesthetized monkeys: Neuronal periodicity and frequency discrimination. J Neurophysiol. 32: 452-484, 1969.

Narselaris T, Merchant H, Amirikian B, Georgopoulos AP. Spatial reconstruction of trajectories of an array of recording microelectrodes. J Neurophysiol. 93: 2318-2330, 2005.

Nicolelis MA, Lebedev MA. Principles of neural ensemble physiology underlying the operation of brain-machine interfaces. Nat Rev Neurosci. 10: 530-540, 2009.

Nieder A, Miller EK. Coding of cognitive magnitude: compressed scaling of numerical information in the primate prefrontal cortex. Neuron. 37: 149-157, 2003.

Oliveira LM, Dimitrov D. Surgical techniques for chronic implantation of microwire arrays in rodents and primates. In: Nicolelis MAL, editor. Methods for Neural Ensemble Recordings. 2nd edition. Boca Raton (FL): CRC Press; 2008. Chapter 2. Frontiers in Neuroscience.

Petkov CI, Kikuchi Y, Milne AE, Mishkin M, Rauschecker JP, Logothetis NK. Different forms of effective connectivity in primate frontotemporal pathways. Nat Commun. 6, 2015.

Peyrache A, Dehghani N, Eskandar EN, Madsen JR, Anderson WS, Donoghue JA, Hochberg LR, Halgren E, Cash SS, Destexhe A. Spatiotemporal dynamics of neocortical excitation and inhibition during human sleep. Proc Natl Acad Sci U S A. 109: 1731-1736, 2012.

Quian Quiroga RQ, Panzeri S. Extracting information from neuronal populations: information theory and decoding approaches. Nat Rev Neurosci. 10: 173-185, 2009.

Romo R, Salinas E. Flutter discrimination: neural codes, perception, memory and decision making. Nat Rev Neurosci. 4: 203-218, 2003.

Rossant C, Kadir SN, Goodman DF, Schulman J, Hunter ML, Saleem AB, Grosmark A, Belluscio M, Denfield GH, Ecker AS, Tolias AS, Solomon S, Buzsáki G, Carandini M, Harris KD. Spike sorting for large, dense electrode arrays. Nat Neurosci. 19: 634-641, 2016.

Royer S, Zemelman BV, Losonczy A, Kim J, Chance F, Magee JC, Buzsáki G. Control of timing, rate and bursts of hippocampal place cells by dendritic and somatic inhibition. Nat Neurosci. 15: 769-775, 2012.

Schmidt S, Horch K, Normann R. Biocompatibility of silicon-based electrode arrays implanted in feline cortical tissue. J Biomed Mater Res. 27: 1393-1399, 1993.

Schultz W, Romo R. Role of primate basal ganglia and frontal cortex in the internal generation of movements. I. Preparatory activity in the anterior striatum. Exp Brain Res. 91: 363-384, 1992.

Schwarz DA, Lebedev MA, Hanson TL, Dimitrov DF, Lehew G, Meloy J, Nicolelis MA. Chronic, wireless recordings of large-scale brain activity in freely moving rhesus monkeys. Nat Methods. 11: 670-676, 2014.

Schwartz AB. Direct cortical representation of drawing. Science. 265: 540-542, 1994.

Seo H, Cai X, Donahue CH, Lee D. Neural correlates of strategic reasoning during competitive games. Science. 346: 340-343, 2014.

Seo M, Lee E, Averbeck BB. Action selection and action value in frontal-striatal circuits. Neuron. 74: 947-960, 2012.

Stark E, Abeles M. Applying resampling methods to neurophysiological data. J Neurosci Meth. 145: 133-144, 2005.

Tolias AS, Sultan F, Augath M, Oeltermann A, Tehovnik EJ, Schiller PH, Logothetis NK. Mapping cortical activity elicited with electrical microstimulation using FMRI in the macaque. Neuron. 48: 901-911, 2005.

Tomita H, Ohbayashi M, Nakahara K, Hasegawa I, Miyashita Y. Top-down signal from prefrontal cortex in executive control of memory retrieval. Nature. 401: 699-703, 1999.

Vandecasteele M, M S, Royer S, Belluscio M, Berényi A, Diba K, Fujisawa S, Grosmark A, Mao D, Mizuseki K, Patel J, Stark E, Sullivan D, Watson B, Buzsáki G. Large-scale recording of neurons by movable silicon probes in behaving rodents. J. Vis. Exp. 61: e3568, 2012.

Ward MP, Rajdev P, Ellison C, Irazoqui PP. Toward a comparison of microelectrodes for acute and chronic recordings. Brain Res. 1282: 183-200, 2009.

Wu F, Stark E, Im M, Cho IJ, Yoon ES, Buzsáki G, Wise KD, Yoon E. An implantable neural probe with monolithically integrated dielectric waveguide and recording electrodes for optogenetics applications. J Neural Eng. 10: 056012, 2013.

Wu F, Stark E, Ku PC, Wise KD, Buzsáki G, Yoon E. Monolithically integrated μLEDs on silicon neural probes for high-resolution optogenetic studies in behaving animals. Neuron. 88: 1136-1148, 2015.

Zarco W, Merchant H, Prado L, Mendez JC. Subsecond timing in primates: comparison of interval production between human subjects and Rhesus monkeys. J Neurophysiol. 102: 3191-3202, 2009.

Figure Legends.

Figure 1. Electrode and microdrive details. A. Schematic drawing (left, center) and view (right) of the Buzsáki64 shank array mounted with high-density connectors manufactured by NeuroNexus. The arrangement of the recording sites at the tip of one shank (left), the array of 8 shanks (center) and the shanks mounted on commercial connectors (right) are shown. B. The probe shown in A (right) is mounted in our custom made microdrive. The movement resolution of the screw is 280 micrometers per turn. C. One shank array similar to that shown in A (left, center) is mounted with a polyamide cable and high-density connectors (NeuroNexus). D. A double microdrive holds two 64 recording site probes with polyamide extensions. This microdrive allows moving independently each probe. Note that the probe connectors are mounted on 'towers' separated from the body of the microdrive and that the two towers and the microdrive are mounted on the same brass basis.

Figure 2. Surgery procedures: skullcap construction. Note that the pictures correspond to a mock surgery. A. The titanium posts, the titanium screws, and the ground and reference screws/wires were fixed to the previously prepared cranium. B. Dental acrylic was employed to cover the cranium, post basis, screws and wires. A flat area (dotted circle) for mounting the microdrive was formed above the implantation site (red asterisk). C. Note the ground and reference wires/pins emerging over the surface of the implant. D. The wires and the base of the ground/reference pins were covered with dental acrylic.

Figure 3. Microdrive implantation. Note that the pictures correspond to a simulated surgery. A. A craniotomy was drilled through the skull cap/scull over the implantation site. B. After opening the dura mater the microdrive was mounted in place by mean of titanium screws and dental acrylic. C. The stainless steel ring is fixed to the skullcap. D. Under microscope assistance, the electrodes were lowered until implanted in the cortex. E. A warm mixture of paraffin/mineral oil was employed to seal the craniotomy. F. The headstage and reference/ground wires were connected to corroborate the presence of neural activity. G. Finally, all connectors were removed and the protective case mounted. H. The behaving monkey. During neural recordings, the head of the monkey was fixed with a standard head holder.

Figure 4. Double microdrive implantation. A. Drawing of the dorsal aspect of the monkey's brain indicating the approximate sites of implantation (red ovals). *PS*: principal sulcus, *ArS*: arcuate sulcus, *CS*: central sulcus B. Close-up of the craniotomy and the mounted microdrive. Before implanting the shanks, the microdrive was attached securely in place by mean of titanium screws and dental acrylic. C. After probe implantation, a mixture of wax and mineral oil serves

to seal the craniotomy. Note the ground and reference pins, previously implanted, protruding from the skullcap. D. The behaving monkey. During neural recordings, the head of the monkey was fixed using a standard head holder. Headstages and ground and reference jumpers are visible.

Figure 5. Recording of large ensembles of pre-SMA cells using a 64-channel silicon probe in a monkey performing the tapping task. A. Broadband recording traces from eight neighboring recording sites (RS1-RS8) in one of the shanks. Extracellular waveforms of seven clustered neurons (spk1-spk7) are superimposed on the traces using the same color code of the spike-discrimination clustering in Figure 6. Calibration: vertical 500 μV; horizontal 10 ms. B. Raster plot of the activity of the seven cells in A using the time stamps and the color code in A. Note that some spikes are present in many of the eight recording sites.

Figure 6. Semi-automatic spike discrimination of the cells. A. Spike clusters of the seven cells depicted in Figure 5 (same color code) displayed along the first principal components of spike waveforms extracted from the 6^{th} and 7^{th} channel. B. Waveforms (mean ± standard deviation) of the seven-clustered cells (spk1-spk7) across the eight neighboring recording sites (RS1-RS8) of one silicon probe. Same color code as in A. C. Calibration: vertical 500 μV; horizontal 1.7 ms. Auto- and Cross-correlograms for all possible pairs of the seven neurons discriminated in A, displayed in a matricial arrangements where the diagonal in color (same color as in A) correspond to the auto-correlations, and the other elements (in gray) are the cross-correlations between different cell pairs. The horizontal line corresponds to a threshold of the 99.9th percentile of a Poisson process defined by the rate resulting from the smoothing procedure (see methods).

Figure 7. A. Raster plot of 64 simultaneously recorded neurons, sorted by their activation phase during the tapping task. B. Projection of the neuronal data of the 64 cells onto its first two principal components revealed a highly constraint population dynamics during the task. C. The neural trajectories of five of the trials in B, color coded for elapsed time since the beginning of the trial (see times on the trial 48 on the right). The open circles depict the seven tapping times, whereas the close triangles the isochronous stimulus times. The rightward arrows illustrate the reward times. Note that the cyclical trajectories of the neural population are similar across trials, even when the monkey produced intervals with different durations (trial 3 = 650ms; 10 = 850 ms; 46 = 750 ms; 48 = 950 ms) or when the monkey perceived the sensory metronome but did not produced taps in synchrony with the stimuli (trial 15).

Figure 8. Identification of putative excitatory pyramidal cells and inhibitory interneurons by clustering of extracellular waveform features. A. Valley-to-peak versus half-peak width values for putative pyramidal cells (blue) and interneurons (red). Data were fitted to a mixture of two Gaussian distributions. Cells were included in the cluster for which their posterior probability >90%. B. Ten superimposed example waveforms for each group. C. Average firing rate for the two groups of cells (bars display SEM.). D. Cross-correlogram between a pyramidal (reference spikes) and an interneuron (target spikes) showing a short latency, narrow peak indicative of a putative mono-synaptic excitatory connections. Red dotted lines indicate 99.9% interval of confidence obtained by jittering the spikes in 10 ms windows. E. Auto-correlograms for the pyramidal (left) and the interneuron (right). The average firing rate is shown on top.

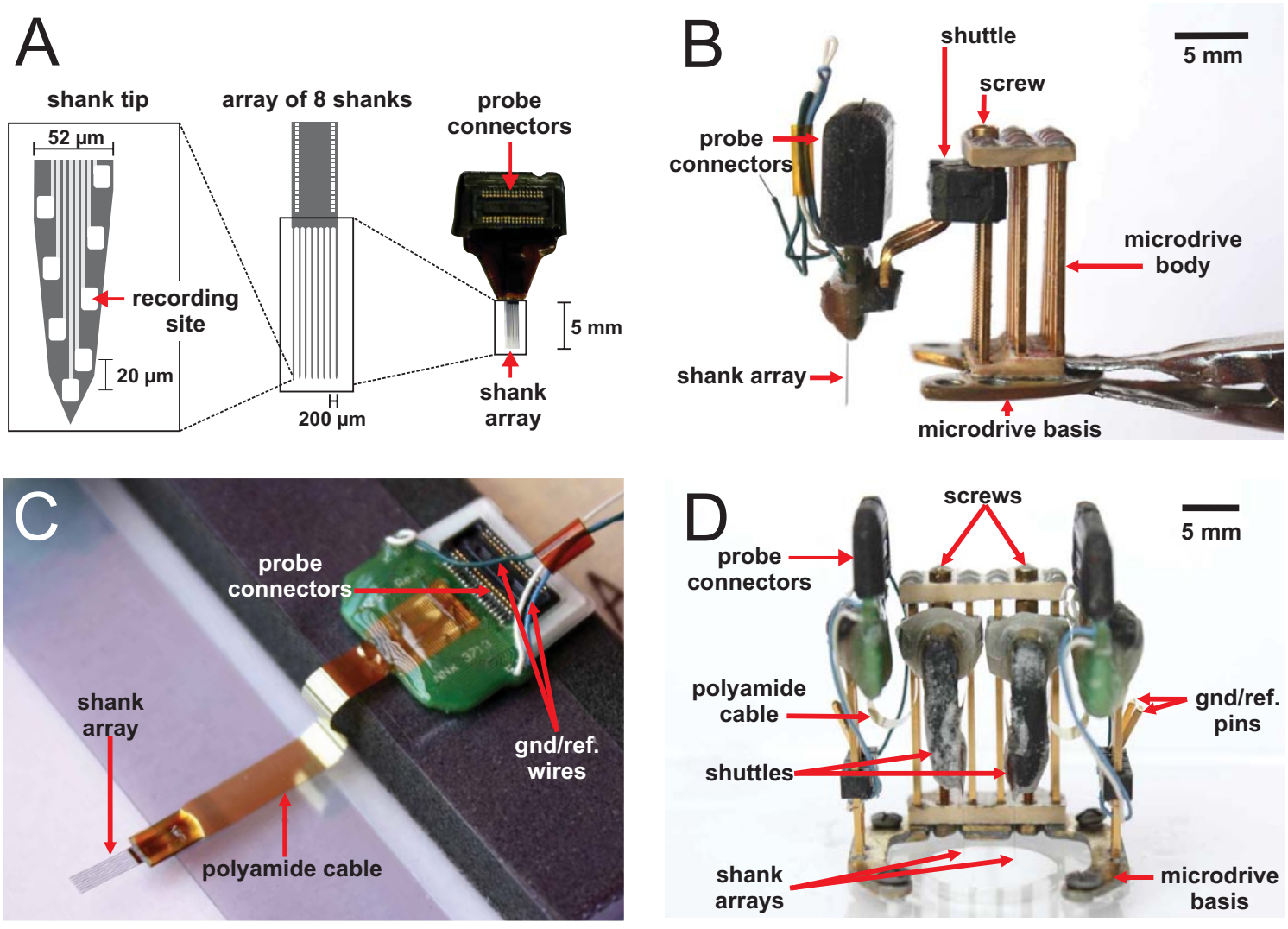
A
shank tip
array of 8 shanks
probe connectors
52 µm
recording site
20 µm
H
200 µm
5 mm
shank array
B
shuttle
screw
5 mm
probe connectors
microdrive body
shank array
microdrive basis
C
probe connectors
shank array
gnd/ref. wires
polyamide cable
D
screws
5 mm
probe connectors
polyamide cable
gnd/ref. pins
shuttles
shank arrays
microdrive basis

Figure 1

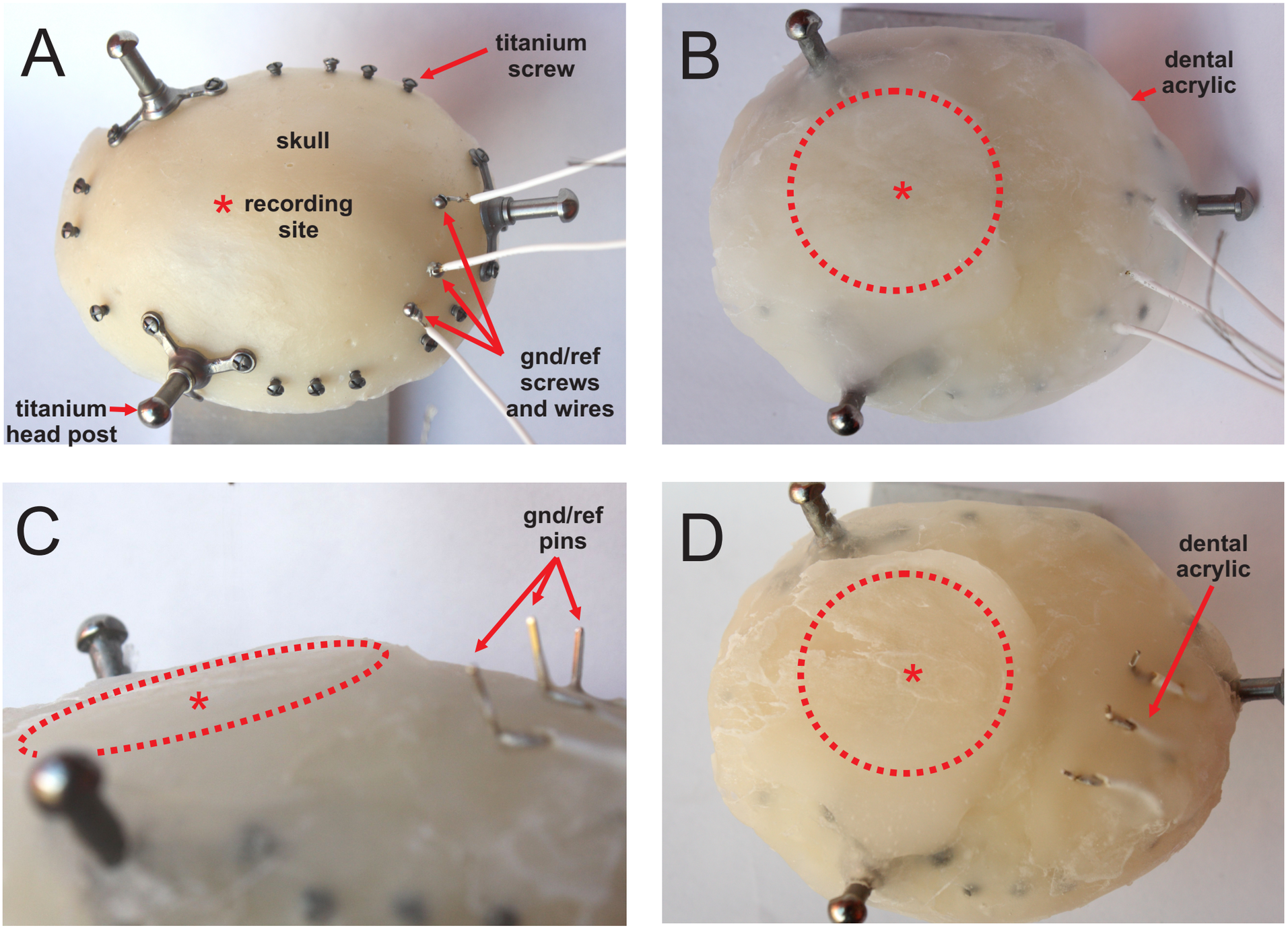
A
titanium screw
skull
recording site
gnd/ref screws and wires
titanium head post
B
dental acrylic
C
gnd/ref pins
D
dental acrylic

Figure 2

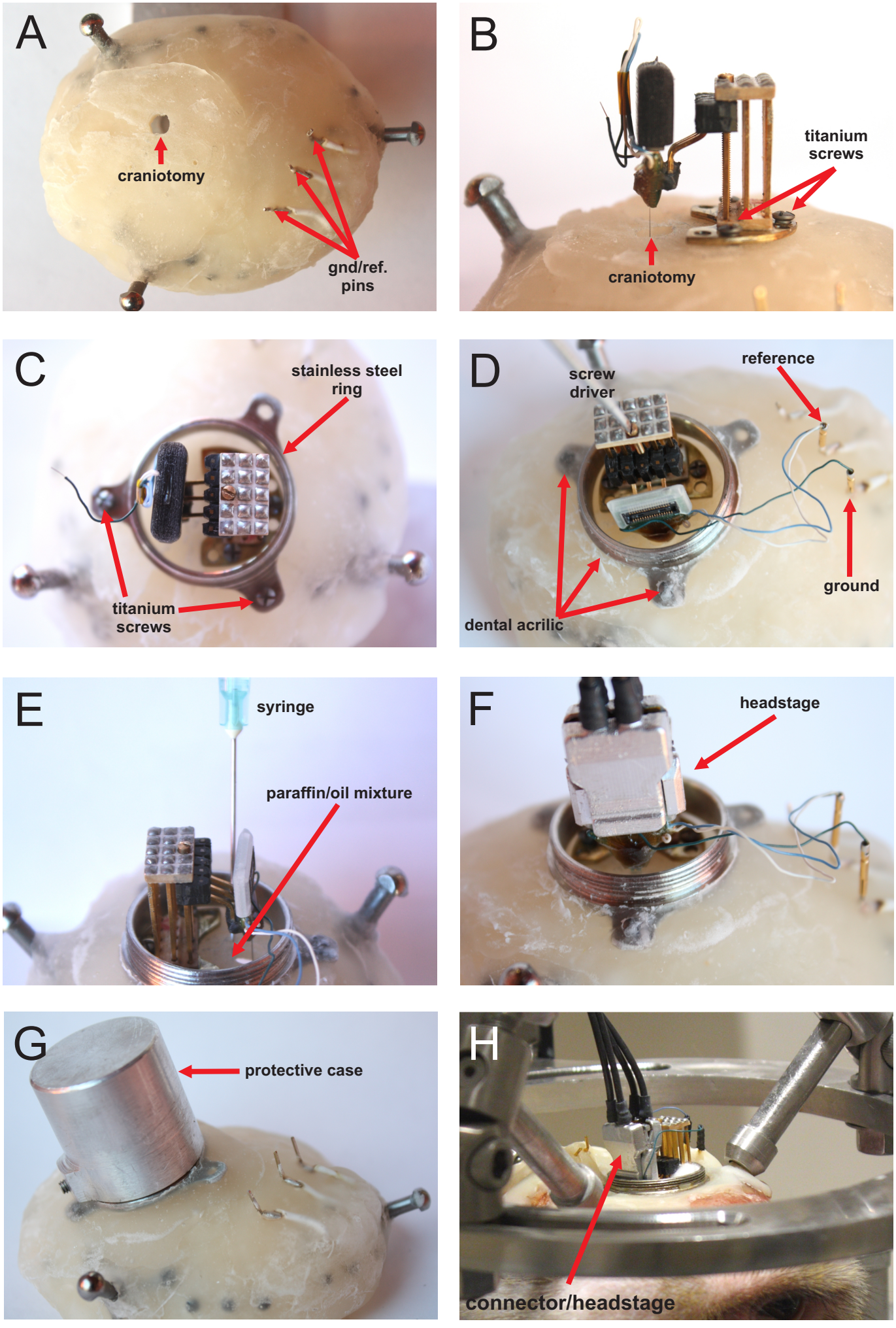
A
craniotomy
gnd/ref.
pins
B
titanium
screws
craniotomy
C
stainless steel
ring
titanium
screws
D
screw
driver
reference
ground
dental acrilic
E
syringe
paraffin/oil mixture
F
headstage
G
protective case
H
connector/headstage

Figure 3

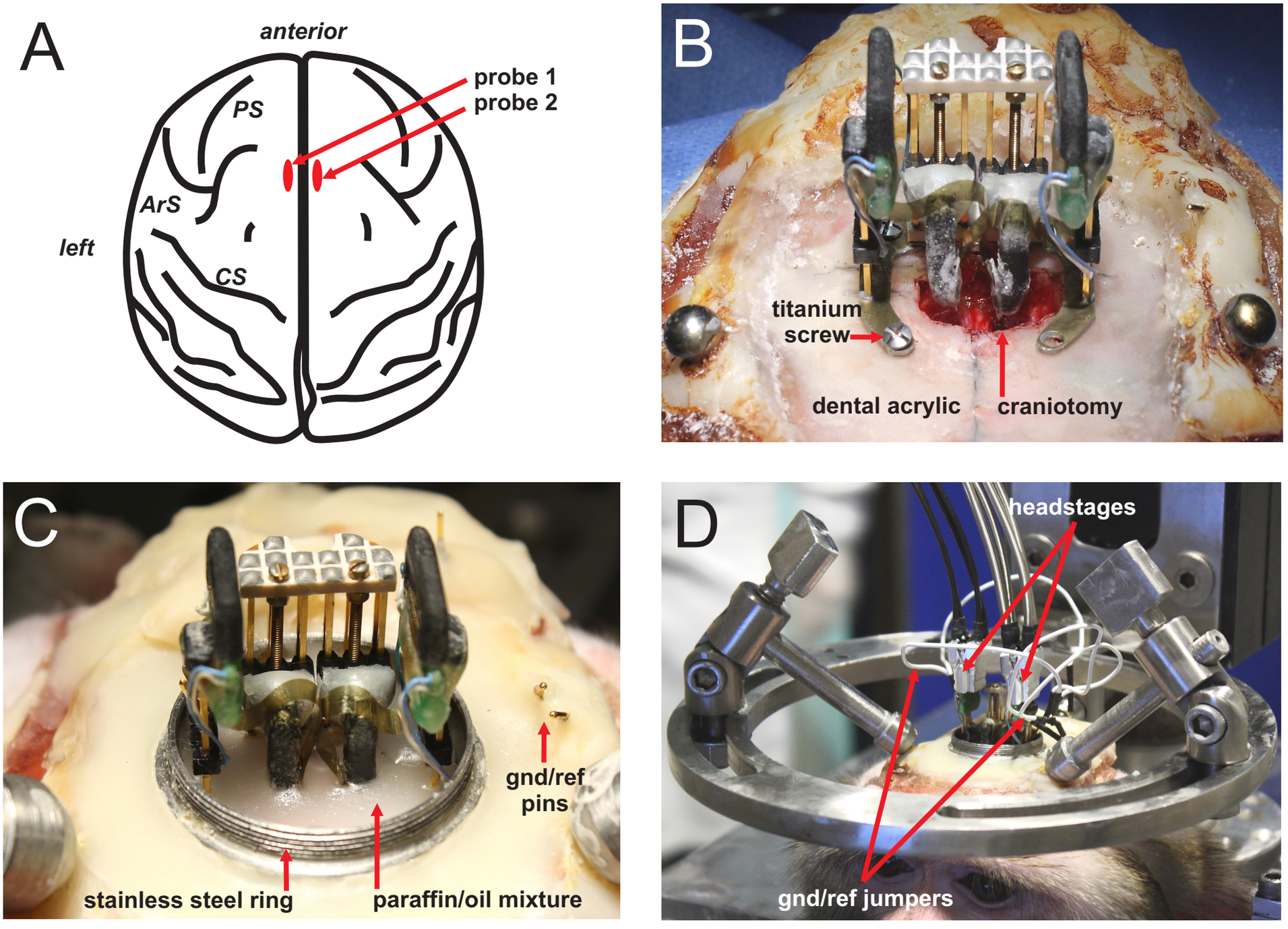
A
anterior
probe 1
probe 2
PS
ArS
left
CS
B
titanium
screw
dental acrylic
craniotomy
C
gnd/ref
pins
stainless steel ring
paraffin/oil mixture
D
headstages
gnd/ref jumpers

Figure 4

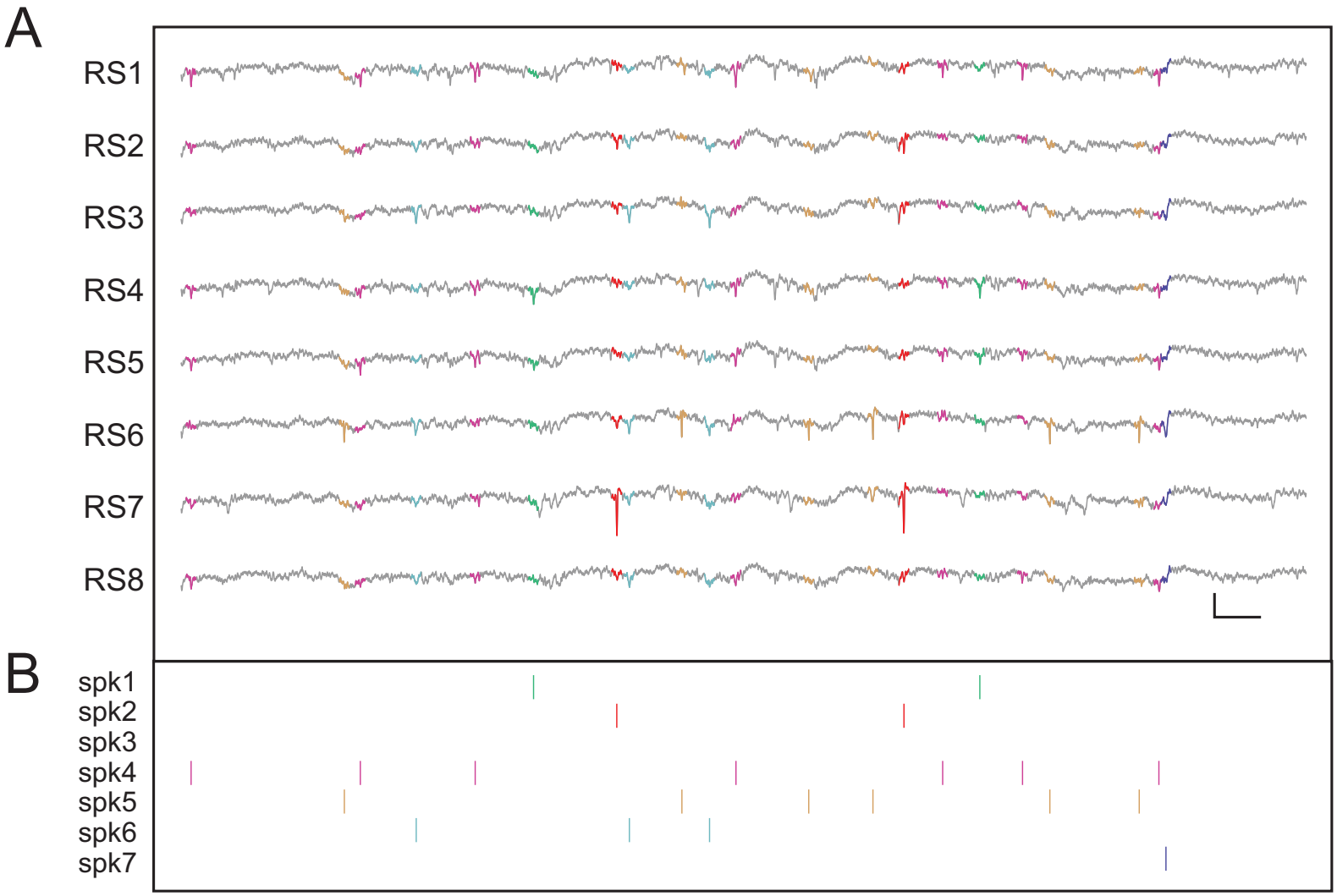
A
RS1
RS2
RS3
RS4
RS5
RS6
RS7
RS8
B
spk1
spk2
spk3
spk4
spk5
spk6
spk7

Figure 5

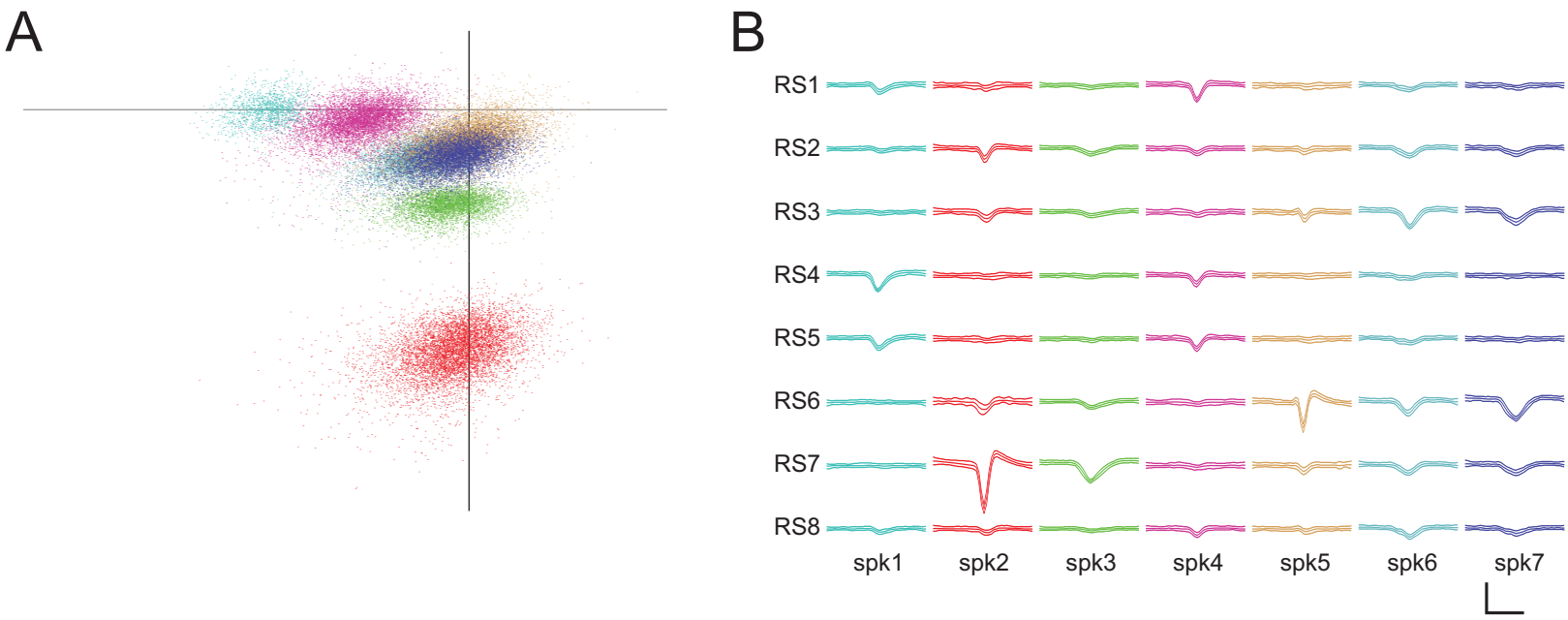
A
B
RS1
RS2
RS3
RS4
RS5
RS6
RS7
RS8
spk1
spk2
spk3
spk4
spk5
spk6
spk7
C
spk1
spk2
spk3
spk4
spk5
spk6
spk7
Discharge rate
Time lag (ms)

Figure 6

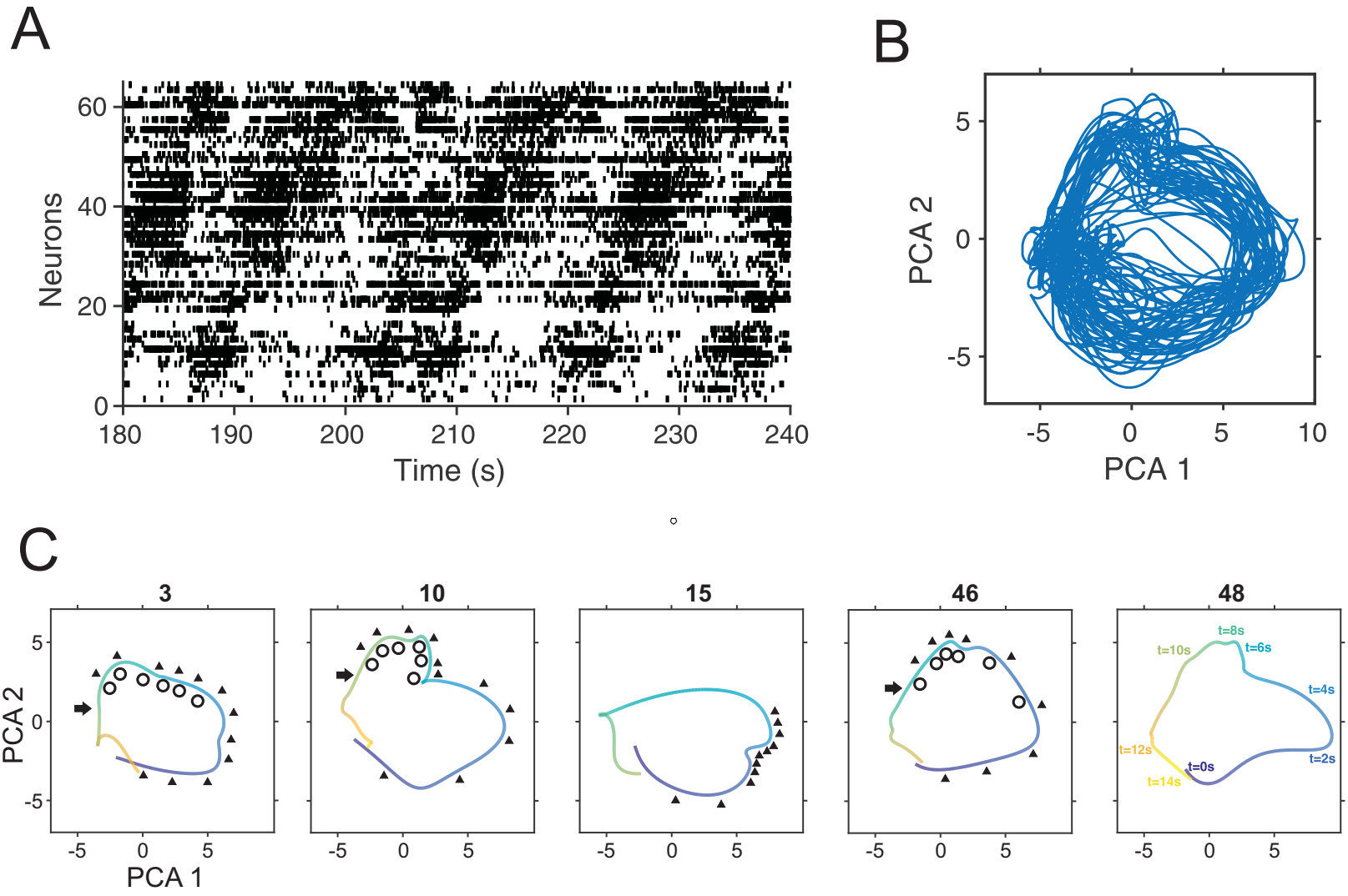
A
Neurons
60
40
20
0
180
190
200
210
220
230
240
Time (s)
B
PCA 2
5
0
-5
-5
0
5
10
PCA 1
C
3
10
15
46
48
PCA 2
PCA 1
t=8s
t=10s
t=6s
t=4s
t=12s
t=0s
t=2s
t=14s

Figure 7

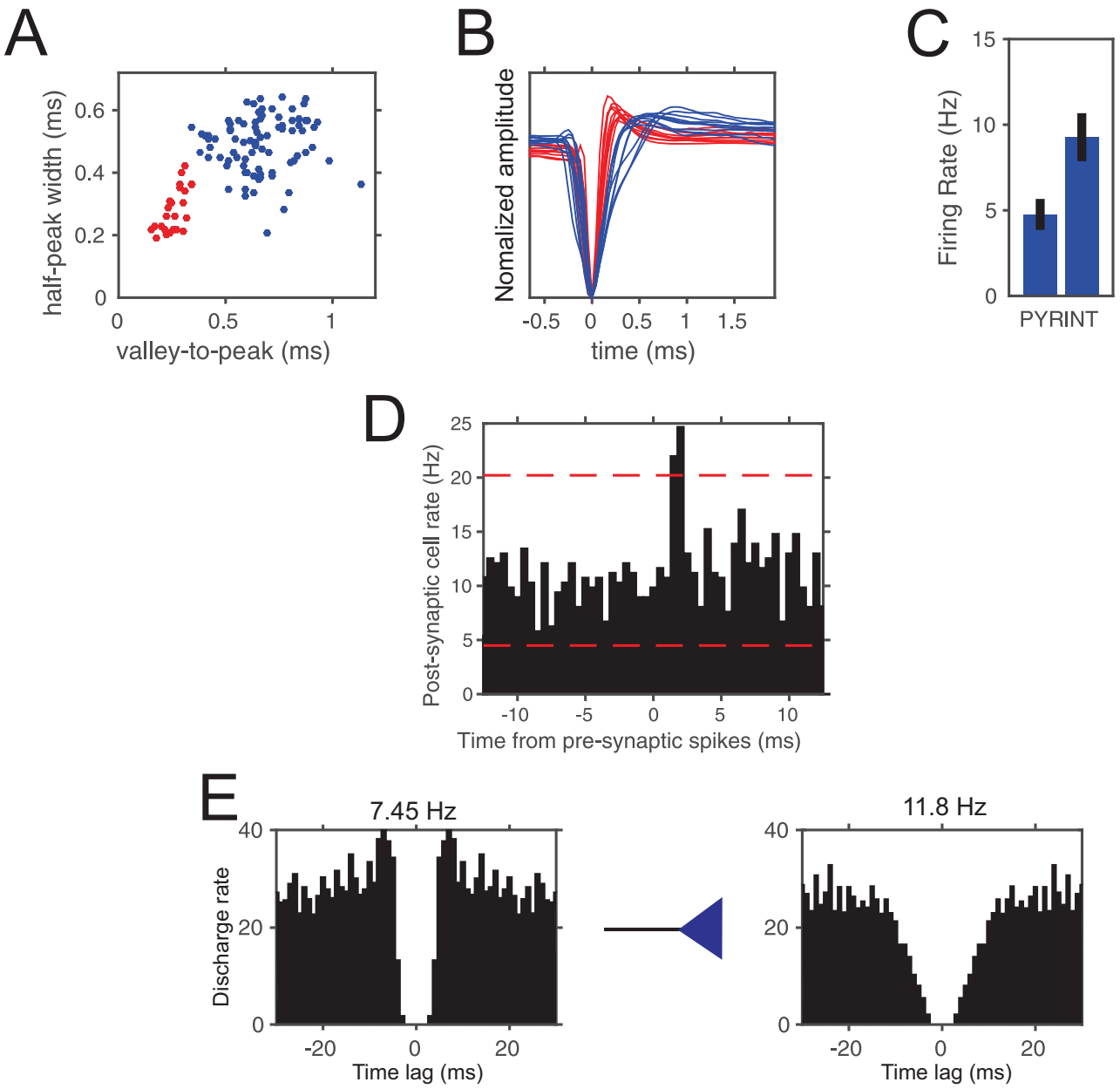
A
half-peak width (ms)
0.6
0.4
0.2
0
0
0.5
1
valley-to-peak (ms)
B
Nomalized amplitude
-0.5
0
0.5
1
1.5
time (ms)
C
Firing Rate (Hz)
15
10
5
0
PYRINT
D
Post-synaptic cell rate (Hz)
25
20
15
10
5
0
-10
-5
0
5
10
Time from pre-synaptic spikes (ms)
E
7.45 Hz
11.8 Hz
Discharge rate
40
20
0
-20
0
20
Time lag (ms)

Figure 8

Table 1. Neural recordings using one of two 64-channel silicon probes in the supplementary motor cortex of a monkey performing a synchronization tapping task.

	Single probe	Double probe
Recording Days	74	72
Recording sessions	62	51
Maximum Depth in mm	4.125	5.12
Total recorded neurons	1905	3862